Chinese Journal of Natural Medicines

Rapid characterization of non-volatile phenolic compounds reveals the reliable chemical markers for authentication of traditional Chinese medicine Xiang-ru among confusing *Elsholtzia* species

Zhen ZENG, Chen ZHANG, Jiadong HU, Feiyan WANG, Ziding WU, Jing WANG, Jun ZHANG, Shuda YANG, Junfeng CHEN, Mingming LI, Qi TONG, Shi QIU, Wansheng CHEN

Citation: Zhen ZENG, Chen ZHANG, Jiadong HU, Feiyan WANG, Ziding WU, Jing WANG, Jun ZHANG, Shuda YANG, Junfeng CHEN, Mingming LI, Qi TONG, Shi QIU, Wansheng CHEN, Rapid characterization of non-volatile phenolic compounds reveals the reliable chemical markers for authentication of traditional Chinese medicine Xiang-ru among confusing *Elsholtzia* species, Chinese Journal of Natural Medicines, 2024, 22(4), 375-384. doi: 10.1016/S1875-5364(24)60614-X.

View online: https://doi.org/10.1016/S1875-5364(24)60614-X

Available online at www.sciencedirect.com
ScienceDirect
Chinese Journal of Natural Medicines 2024, **22**(4): 375-384
doi: 10.1016/S1875-5364(24)60614-X
Chinese Journal of Natural Medicines

•Original article•

Rapid characterization of non-volatile phenolic compounds reveals the reliable chemical markers for authentication of traditional Chinese medicine Xiang-ru among confusing *Elsholtzia* species

ZENG Zhen[1Δ], ZHANG Chen[1Δ], HU Jiadong[1, 2Δ], WANG Feiyan[1], WU Ziding[1], WANG Jing[1], ZHANG Jun[3], YANG Shuda[4], CHEN Junfeng[1], LI Mingming[2], TONG Qi[1], QIU Shi[1, 5*], CHEN Wansheng[1, 2*]

[1] *The SATCM Key Laboratory for New Resources & Quality Evaluation of Chinese Medicine, Institute of Chinese Materia Medica, Shanghai University of Traditional Chinese Medicine, Shanghai 201203, China;*
[2] *Department of Pharmacy, Second Affiliated Hospital of Navy Medical University, Shanghai 200003, China;*
[3] *Kunming Plant Classification Biotechnology Co., Ltd., Kunming 650500, China;*
[4] *School of Pharmaceutical Sciences and Yunnan Key Laboratory of Pharmacology for Natural Products, Kunming Medical University, Kunming 650500, China;*
[5] *State Key Laboratory for Quality Ensurance and Sustainable Use of Dao-di Herbs, Beijing, 100700, China*

Available online 20 Apr., 2024

[ABSTRACT] The aerial parts of *Mosla chinensis* Maxim. and *Mosla chinensis* cv. 'Jiangxiangru' (MCJ) are widely utilized in traditional Chinese medicine (TCM), known collectively as Xiang-ru. However, due to clinical effectiveness concerns and frequent misidentification, the original plants have increasingly been substituted by various species within the genera *Elsholtzia* and *Mosla*. The challenge in distinguishing between these genera arises from their similar morphological and metabolic profiles. To address this issue, our study introduced a rapid method for metabolic characterization, employing high-resolution mass spectrometry-based metabolomics. Through detailed biosynthetic and chemometric analyses, we pinpointed five phenolic compounds—salviaflaside, cynaroside, scutellarein-7-*O*-D-glucoside, rutin, and vicenin-2—among 203 identified compounds, as reliable chemical markers for distinguishing Xiang-ru from closely related Elsholtzia species. This methodology holds promise for broad application in the analysis of plant aerial parts, especially in verifying the authenticity of aromatic traditional medicinal plants. Our findings underscore the importance of non-volatile compounds as dependable chemical markers in the authentication process of aromatic traditional medicinal plants.

[KEY WORDS] Genus *Elsholtzia*; Genus *Mosla*; Traditional Chinese medicine; Xiang-ru; Non-volatile phenolic compounds; Liquid chromatography-mass spectrometry

[CLC Number] R917 **[Document code]** A **[Article ID]** 2095-6975(2024)04-0375-10

Introduction

Traditional Chinese medicine Xiang-ru (TCM-XR), specifically the aerial parts of *Mosla chinensis* Maxim. and MCJ is renowned for its astringent, antipyretic, and antiviral properties [1]. Additionally, it serves as a wild vegetable and is incorporated into food as additives [2]. TCM-XR has been an integral part of Chinese medicinal practices, primarily as the chief herb in the historic prescription 'Xin-Jia-Xiang-Ru-Yin', which has been employed since the Qing dynasty to address the summer cold syndrome [3]. However, the plant origins of Xiang-ru have experienced varietal shifts, incorporating multiple species from the *Mosla* and *Elsholtzia* genera, leading to confusion in accurately identifying the original plants [4]. This confusion is exacerbated by the similar morphologies and applications of *Elsholtzia and Mosla*, to the extent that the wrong species, *Elsholtzia splendens*, was in-

[Received on] 21-Aug.-2023
[Research funding] This work was supported by the National Key R&D Program of China (No. 2022YFC3501700), the Young Elite Scientists Sponsorship Program by Cast (No. 2021-QNRC1-02), the Key Project at Central Government Level: The Ability Establishment of Sustainable Use for Valuable Chinese Medicine Resources (No. 2060302), and the Research Project of Science and Technology Commission of Shanghai Municipalit (No. 21DZ2202300).
[*Corresponding author] E-mails: davidhugh@msn.com (QIU Shi); chenwansheng@shutcm.edu.cn (CHEN Wansheng)
[Δ]These authors contributed equally to this work.
These authors have no conflict of interest to declare.

cluded in earlier editions of the Chinese Pharmacopoeia [5-7]. Furthermore, the aerial parts of *E. ciliata* are recognized in the Korean Pharmacopoeia and have been traditionally used to treat a range of conditions, including respiratory diseases, fever, headache, diarrhea, dysentery, indigestion, and edema [8]. Given the similar pharmacological effects and clinical applications of both genera, discerning the chemical differences between them is vital for correctly identifying the original plants and effectively utilizing plant resources.

Current research on the *Elsholtzia* and *Mosla* genera has predominantly concentrated on analyzing their volatile oils, which are recognized for their antibacterial and antioxidant capabilities, including substances like elsholtzia ketone, carvacrol, and thymol [9, 10]. Nevertheless, the assessment of these volatile components in dried samples of TCM-XR and commercially available products poses challenges due to their inherent volatility. This characteristic significantly affects the accuracy of detection, rendering it highly contingent upon the freshness of the samples [11]. In contrast, non-volatile phenolic compounds, which are also abundantly present in both *Elsholtzia* and *Mosla*, demonstrate greater stability. These primarily include flavonoids and organic acids, offering distinct advantages for the application and analysis in dried forms, such as decoction pieces and commercial products, due to their relative stability [12, 13]. Despite this, reports on the non-volatile components within the *Elsholtzia* and *Mosla* genera remain scarce, even though such non-volatile phenolic compounds frequently occur in the aerial parts of plants. These compounds are crucial for characterizing phytochemical profiles, differentiating between plant species, and exploring chemical diversity [14].

Studies of the plant metabolome present considerable challenges, attributable to the vast diversity of chemical classes, the wide range of metabolite concentrations, and the complexity inherent in plant materials [15]. The integration of chromatographic separation with high-resolution mass spectrometry (MS) has emerged as a highly sensitive technique for metabolite identification, offering more accurate structural insights and extensive metabolomics data [16]. The use of liquid chromatography-MS (LC-MS) analysis provides an effective and precise method for distinguishing specific metabolites, which has substantially increased the volume of metabolomics research [17]. Chemical markers are essential for the quality control (QC) of Traditional Chinese Medicine (TCM), enabling the differentiation between adulterated and authentic samples, thereby guaranteeing their consistency, safety, and efficacy [18]. Metabolomics approaches are now instrumental in identifying chemical markers and elucidating the relationships between chemical compounds and plant species. This offers valuable perspectives on interspecies variations and phytochemical diversity [19]. For TCM characterized by aromatic aerial parts, it is crucial to employ robust chemical markers throughout the development and manufacturing stages to assure the internal quality and veracity of the original plants.

In this study, we examined eight representative species, which included two *Mosla* species (*M. chinensis* (MC) and MCJ and six *Elsholtzia* species (*E. ciliate*, *E. blanda*, *E. fruticose*, *E. rugulosa*, *E. splendens*, and *E. kachinensis*). We developed an analytical strategy for high-throughput chemical characterization, enabling the rapid classification and identification of non-volatile phenolic metabolites. This approach utilized metabolomics and fragmentation patterns under high-energy positive-ion mode. Through this method, we were able to screen for reliable chemical markers that distinguish TCM-XR from species that are easily confused, such as *E. ciliata* and *E. splendens*, which have historically been mistaken for the original plants of TCM-XR.

Experimental

Materials and chemicals

Eight species from two genera were sourced from various locations across China, specifically Yunnan, Jiangxi, Hubei, and Zhejiang Provinces. These included MC, MCJ, *E. splendens* (ES), *E. ciliate* (EC), *E. kachinensis* (EK), *E. rugulosa* (ER), *E. blanda* (EB), and *E. fruticose* (EF). Prof. YANG Shuda of Kunming Medical University confirmed the identity of all plant samples. A voucher specimen for each species was deposited at the Institute of Chinese Materia Medica, Shanghai University of TCM. Detailed documentation of the collected samples is available in Table S1 and Figure S1. Additionally, three batches of TCM-XR (TCM-XR-1, TCM-XR-2, and TCM-XR-3) products were acquired from herbal markets across different provinces in China, as detailed in Table S1 and illustrated in Figure S2.

Acetonitrile and methanol (HPLC grade) were purchased from Merck (Darmstadt, Germany). Formic acid (HPLC grade) was purchased from Fisher Scientific (Fair Lawn, NJ, USA). Pure distilled water was obtained from Watsons Water (Hong Kong, China). Warfarin was obtained from Sigma-Aldrich (Madrid, Spain). The following reference standards were purchased from Shanghai Standard Technology (Shanghai, China): vicenin-2 (**1**), schaftoside (**2**), vicenin-3 (**3**), vitexin-4"-*O*-glucoside (**4**), vitexin (**5**), violanthin (**6**), isovitexin (**7**), apioside (**8**), apigenin 7-*O*-*β*-D-glucuronide (**9**), apigenin-7-glucoside (**10**), tilianin (**11**), apigenin (**12**), acacetin (**13**), genkwanin (**14**), homoorientin (**15**), orientin (**16**), luteolin-7-*O*-*β*-D-glucuronide (**17**), cynaroside (**18**), isoscoparin (**19**), diosmin (**20**), luteolin 3'-glucuronide (**21**), luteolin (**22**), chrysoeriol (**23**), diosmetin (**24**), hydroxygenkwanin (**25**), pilloin (**26**), astragalin 7-*O*-*β*-D-glucopyranoside (**27**), kaempferol 3-*O*-sophroside (**28**), kaempferol 3-gentiobioside (**29**), kaempferol 3-*O*-neohesperidoside (**30**), kaempferol-3-glucorhamnoside (**31**), kaempferol-3-*O*-rutinoside (**32**), kaempferitrin (**33**), kaempferol 3-*O*-*β*-D-glucuronide (**34**), astragalin (**35**), kaempferol 7-*O*-*β*-D-glucoside (**36**), juglalin (**37**), complanatoside (**38**), kaempferol-3-*O*-rhamnoside (**39**), kaempferol (**40**), kaempferide (**41**), rutin (**42**), hyperoside (**43**), quercetin 3-*O*-*β*-D-glucuronide (**44**), quercetin 7-*O*-*β*-D-glucopyranoside (**45**), quercetin 3-*O*-*β*-D-

xylopyranoside (**46**), guaijaverin (**47**), quercitrin (**48**), isorhamnetin-3-*O*-*β*-D-glucoside (**49**), isoquercitrin (**50**), vincetoxicoside B (**51**), quercetin (**52**), isorhamnetin (**53**), tamarixetin (**54**), protocatechuic acid (**55**), 2,5-dihydroxybenzoic acid (**56**), 4-hydroxybenzoic acid (**57**), vanillic acid (**58**), isovanillic acid (**59**), syringic acid (**60**), 2-hydroxy-6-methoxybenzoic acid (**61**), 4-methoxysalicylic acid (**62**), caffeic acid (**63**), *trans*-*p*-coumaric acid (**64**), ferulic acid (**65**), sinapic acid (**66**), isoferulic acid (**67**), aesculetin (**68**), 7-hydroxycoumarin (**69**), 3,4-dihydroxyphenylacetic acid (**70**), danshensu (**71**), rosmarinic acid (**72**), salvianolic acid E (**73**), salvianolic acid B (**74**), D-(–)-quinic acid (**75**), neochlorogenic (**76**), chlorogenic acid (**77**), cryptochlorogenic acid (**78**), isochlorogenic acid B (**79**), 3,5-di-*O*-caffeoylquinic acid (**80**), 4,5-dicaffeoylquinic acid (**81**).

Sample preparation for LC-MS

Each plant was sectioned into stem and leaf portions. These portions, including whole plant samples, were immediately frozen in liquid nitrogen, then pulverized into fine powders and sifted through a 40 mesh sieve to ensure homogeneity. The resulting powders (0.01 g) were then subjected to extraction using 1 mL of 70% methanol (*V*/*V*), which included warfarin at a concentration of 5 μg·mL^{-1} as an internal standard. This extraction process was carried out for 1 h in an ultrasonic bath operating at 53 kHz and 350 W, at room temperature. Following the extraction, the samples were centrifuged at 14 500 × *g* for 15 min at room temperature. The supernatants were collected and stored at 4 °C until further analysis by UHPLC-QTOF-MS. To monitor the performance and potential drift of the UHPLC-QTOF-MS system over time, a QC sample was prepared by amalgamating 20 μL from each individual sample. This pooled QC sample was analyzed alongside the individual samples to ensure the accuracy and reliability of the analytical procedure.

LC-MS analysis

The analysis was conducted utilizing an ACQUITY UPLC system (Waters), equipped with a binary pump, autosampler, and column compartment. The separation of analytes within each sample was achieved on an ACQUITY UPLC T3 column (2.1 mm × 100 mm, 1.8 μm) maintained at a constant temperature of 40 °C. The mobile phases consisted of solvent A (0.1% *V*/*V* formic acid in water) and solvent B (0.1% *V*/*V* formic acid in acetonitrile). The gradient elution was programmed as follows: an increase from 2% to 20% B from 0 to 7 min; 20% to 22% B from 7 to 11 min; 22% to 60% B from 11 to 20 min; 60% to 65% B from 20 to 25 min; 65% to 95% B from 28 to 30 min; held at 95% B from 30 to 33 min; followed by a re-equilibration to 2% B for 3 min. The injection volume was set at 2 μL with a flow rate of 0.40 mL·min^{-1}.

The UPLC system was integrated with a Waters Xevo G2-XS QTOF mass spectrometer, featuring an electrospray ionization source. The instrument settings for MS included a sample cone voltage of 30 V, a source temperature of 150 °C, a desolvation temperature of 450 °C, a cone gas flow of 50 L·h^{-1}, a desolvation gas flow of 600 L·h^{-1}, and a capillary voltage of 2.5 kV for negative-ion mode or 3 kV for positive-ion mode. The mass spectrometer was programmed to scan a mass range of 50–1200 with a scan time of 0.35 s. The collision energy settings were low at 6 eV for negative-ion mode and 45 eV for positive-ion mode, with high collision energy ramping from 60 to 80 eV for both modes. Leucine enkephalin (200 pg·L^{-1}) served as an external reference for mass accuracy during data acquisition, while sodium formate (0.5 mmol·L^{-1}) was used for instrument calibration. Data interpretation was facilitated by MassLynx v.4.2 software (Waters).

Data processing

The raw MS data, collected in centroid mode, were initially converted into the Analysis Base File (ABF) format using the ABF Converter (https://www.reifycs.com/AbfConverter/). Subsequently, the data were imported into MS-DIAL version 4.90 (http://prime.psc.riken.jp/compms/msdial/main.html) for analysis [20]. The analysis parameters were set as follows: MS^1 tolerance at 0.01 Da; MS^2 tolerance at 0.02 Da; retention time range from 0.6 to 21 minutes; MS^1 and MS/MS mass ranges from 100 to 1000; minimum peak height at 5000; mass slice width at 0.1 Da; and MS/MS abundance cut off at 2,000 amplitude. The retention time tolerance was maintained at 0.15 min. For the negative-ion mode, the selected adduct types included $[M - H]^-$, $[M + HCOO]^-$, $[M + Na - 2H]^-$, $[M + K - 2H]^-$, $[M + Cl]^-$, $[2M - H]^-$, and $[2M + FA - H]^-$, whereas for the positive-ion mode, the adduct types were $[M + H]^+$, $[M + Na]^+$, $[M + K]^+$, $[M + NH4]^+$, and $[2M + H]^+$. Peak tables produced by MS-DIAL were then refined and clustered using MS-CleanR (https://github.com/eMetabo-HUB/MS-CleanR) [21] with specified parameters: a minimum blank ratio of 0.8; a maximum relative standard deviation of 30; a RMD range of 80–320; a maximum mass difference of 0.005 Da; and a maximum retention time difference of 0.03 min. A correlation was deemed statistically significant with a Pearson correlation coefficient ≥ 0.8 and an α value set at 0.05. The most intense feature within each cluster was selected to create the final peak table, which was used for metabolite identification.

Chemometric analysis

In this study, each sample extract was normalized using warfarin (5 g·mL^{-1}) as the internal standard, employing the method processed in MS-DIAL for normalization. The normalized metabolomics data were subsequently imported into SIMCA-P 14.1 (Umetrics AB, Umea, Sweden) software. Principal Component Analysis (PCA) was applied to explore unsupervised pattern recognition across different species. To further identify potential chemical markers, Orthogonal Partial Least Squares-Discriminant Analysis (OPLS-DA) was conducted for defined groups (n = 2), facilitating supervised pattern recognition. In the OPLS-DA model, metabolites exhibiting a Variable Importance in Projection (VIP) value greater than 1.0 and a P value less than 0.05 were identified

as potential chemical markers, reflecting their significant contribution to the model.

Results and Discussion

Workflow for rapid characterization of non-volatile phenolic compounds.

A workflow was designed for the rapid classification and characterization of non-volatile phenolic metabolites across different plant species. Illustrated in Fig. 1, the workflow begins with the acquisition of raw data from plant samples and their corresponding reference standards, employing both positive-ion and negative-ion modes for analysis. In negative-ion mode, the MS^1 and MS^2 mass spectra are pivotal for identifying quasi-molecular ions and their common fragment ions, respectively. The application of high collision energy in positive-ion mode is strategically used to elucidate diagnostic product ions, facilitating the rapid classification of quasi-molecular ions similarly detected in negative-ion mode. This approach significantly enhances the efficiency of chemical classification by yielding distinct fragmentation patterns and diagnostic product ions.

Peak detection, alignment, and normalization procedures were executed utilizing the MS-DIAL software, facilitating the generation of a comprehensive peak table aimed at maximizing the detection of phenolic metabolites. Subsequently, this peak table underwent filtration *via* the MS-CleanR tool, employing a relative mass defect (RMD) filter with settings adjusted to 80–320, to enhance the exploration of phenolic metabolites. The refined peak table thus contributed to the accurate identification of metabolites and facilitated subsequent chemometric analyses. By integrating metabolomic methodologies with the distinct mass-spectral signatures observed between negative- and positive-ion modes, a broad spectrum of phenolic metabolites was identified, encompassing both known and previously unknown phenolic compounds.

Rapid classification and characterization of non-volatile phenolic compounds

In this study, 121 samples underwent analysis via UHPLC-QTOF-MS, utilizing both negative and positive ion modes. These samples comprised 104 plant organ specimens from the *Elsholtzia* and *Mosla* genera, alongside 17 TCM-XR products sourced from three distinct batches (TCM-XR-1, TCM-XR-2, and TCM-XR-3, detailed in Table S2). The total ion chromatograms (TIC) generated through this analysis exhibited similar profiles, making it challenging to distinguish among the eight species studied (refer to Figs. S3−S4). To en-

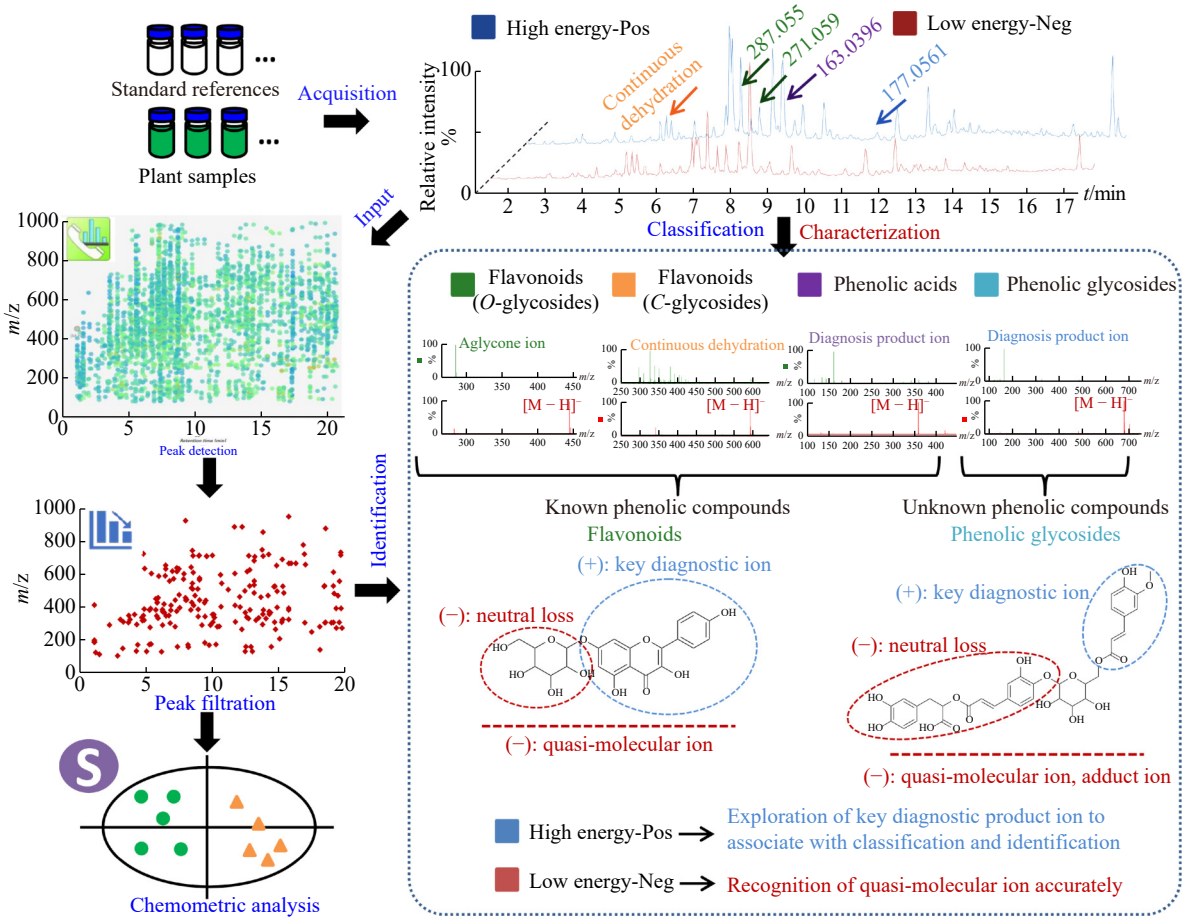

Fig. 1 The established workflow based on metabolomics approach and MS (high-energy positive-ion mode) for rapid characterization of non-volatile phenolic compounds in plants.

hance the detection and differentiation of both known and unknown phenolic compounds, 81 phenolic reference standards spanning three chemical classes were employed. This strategy facilitated the establishment of correlations between retention times and their corresponding molecular structures (as documented in Table S2 and Fig. S5). The elution behaviors of select phenolic compounds were analyzed, focusing on the influence of caffeoyl groups, methoxy groups, and glycosidic linkages on their chromatographic behaviors, as demonstrated in Fig. 2A. Typically, LC-MS analysis presents challenges in pinpointing substituent conjunction sites; however, examining the interplay between retention times and structural features significantly enhances the capacity to distinguish between isomeric compounds sharing the same phenolic aglycone base (illustrated in Table S2 and Fig. S5). For example, Luteolin-7-*O*-glycoside (cynaroside, 7.35 min) exhibited earlier elution than its 3′-*O*-glycoside counterpart (luteolin 3′-*O*-glucuronide, 8.92 min), with both compounds eluting after the 3-*O*-glycoside variant, such as kaempferol-7-*O*-*β*-D-glucoside (8.25 min) compared to astragalin (kaempferol-3-*O*-*β*-D-glucoside, 8.04 min). This elution pattern analysis facilitates the identification of flavonoid glycosides' conjunction sites (as shown in Fig. S5). Consequently, 36 reference standards were detected, with their distribution patterns across the stems and leaves of the eight species illustrated in Fig. 2B. The findings reveal that while three phenolic compound groups exhibited similar distribution patterns in both plant organs, the majority of metabolites presented in higher concentrations within the leaves.

The chemical classification of phenolic compounds was effectively achieved through the analysis of MS patterns, utilizing a combination of negative and positive ion modes under high energy. For instance, flavonoid-*O*-glycosides exhibited consistent diagnostic fragments across MS^2 in both negative and positive ion modes, allowing for the direct investigation of the flavonoid aglycone (Fig. 3A). Conversely, flavonoid-*C*-glycosides demonstrated a distinct behavior in positive ion mode, characterized by continuous dehydration (Fig. 3B). A diagnostic fragment with *m/z* 163.04, identified in positive ion mode, was indicative of phenolic and quinic acid derivatives featuring caffeoyl substructures (Figs. 3C and 3D). Furthermore, fragments with *m/z* 197.04 and 191.05 in negative ion mode suggested the presence of danshensu and quinic acid substructures, respectively (Figs. 3C and 3D). Diagnostic product ions observed in positive ion mode at high energy were instrumental in identifying previously unknown phenolic compounds. A quasi-molecular ion with *m/z* 697.18 (compound **184**) displayed a neutral loss of 198.05 and product ions with *m/z* 359.07, 179.03, and 161.06, hinting at substructures such as rosmarinic acid and a glucose moiety (Fig. 3E). Additionally, the diagnostic product ion *m/z* 177.05, identified specifically in positive ion mode, indicated the existence of a ferulic acid-like substructure (Fig. 3E). By correlating substructure data from both ion modes with structural searches in the SciFinder database, a tentative structure for *m/z* 697.18 was proposed (Fig. 3E). Fig. 3F illustrates how this workflow enabled the rapid classification of chemical classes by comparing MS patterns in negative and positive ion modes. Following this approach and guided by the generated peak table, 203 phenolic compounds were identified across the eight studied species of *Elsholtzia* and *Mosla*, predominantly consisting of phenolic acids, phenolic glycosides, and flavonoids (Table S3). This workflow and analytical strategy are anticipated to have broad applicability in the study of aerial parts for a wide range of plant samples, enhancing the efficiency and depth of phytochemical investigations.

Chemical differentiation between Elsholtzia and Mosla

Following the comprehensive chemical characterization, chemometric analysis was performed to explore the metabolic variations among the selected species of *Elsholtzia* and *Mosla*. An unsupervised PCA specifically focused on the leaf and stem organs in negative-ion mode, was conducted to visualize the metabolic disparities across the eight species. Notably, the metabolite distribution in leaf samples from EB and EF was significantly distinct, falling outside the confidence interval. This pronounced difference was similarly observed in the stem samples, as illustrated in Fig. 4A. In efforts to refine the differentiation between *Elsholtzia* and *Mosla* species, two species (EB and EF), which exhibited clear discrepancies, were omitted from the subsequent analysis, as depicted in Fig. 4B. This strategic exclusion revealed a closer clustering among two *Elsholtzia* species (EC and ES) and MCJ, which were previously misidentified as original TCM-XR plants. The outcomes of the PCA closely aligned with the results from phylogenetic tree analysis (Fig. S6), affirming the efficacy of this metabolomic strategy in accurately authenticating the species in question. This approach not only underscores the potential of metabolomic analyses in distinguishing closely related species but also highlights the importance of targeted chemometric evaluations in resolving taxonomic ambiguities, thereby supporting the accurate identification and authentication of medicinal plant species.

Supervised OPLS-DA models were employed to delineate the metabolic markers distinguishing *Elsholtzia* from *Mosla*, with reference to the sample configurations illustrated in Figures S7A and S7C. The S-plots, as depicted in Figures S7B and S7D, revealed similar differential metabolites distributed around the periphery of the variables. This pattern suggests that the metabolic distinctions between *Elsholtzia* and *Mosla* were primarily attributed to variations in the concentrations of metabolic markers, rather than the exclusive presence of specific metabolites in EB and EF. A Student's *t*-test was applied to identify chemical markers distinguishing the two genera, adhering to criteria of VIP greater than 1.0 and *P*-value less than 0.05. Utilizing these parameters, 31 and 33 metabolic markers were pinpointed for the models represented in Figures S7B and S7D, respectively, as catalogued in Tables S4 and S5. Notably, 27 metabolic markers were consistently identified across both models. These included a range of phenolic and flavonoid glycosides, thereby affirming their reliability as chemical markers for differentiat-

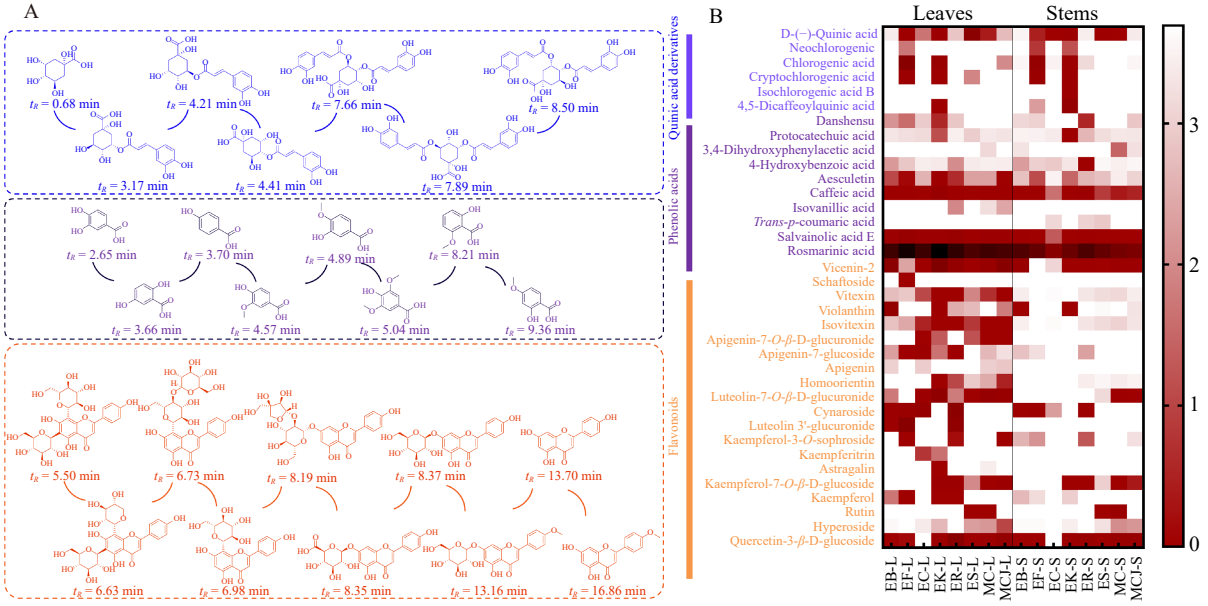

Fig. 2 The relationships of "structure-elution" and the distribution of phenolic reference standards in leaves and stems of *Elsholtzia* and *Mosla* species. (A) The elution patterns of three classes of phenolic reference standards in the negative-ion mode; (B) A heat-map presents the relative content of detected phenlic reference standards in leaves and stems of *Elsholtzia* and *Mosla* species in the negative-ion mode.

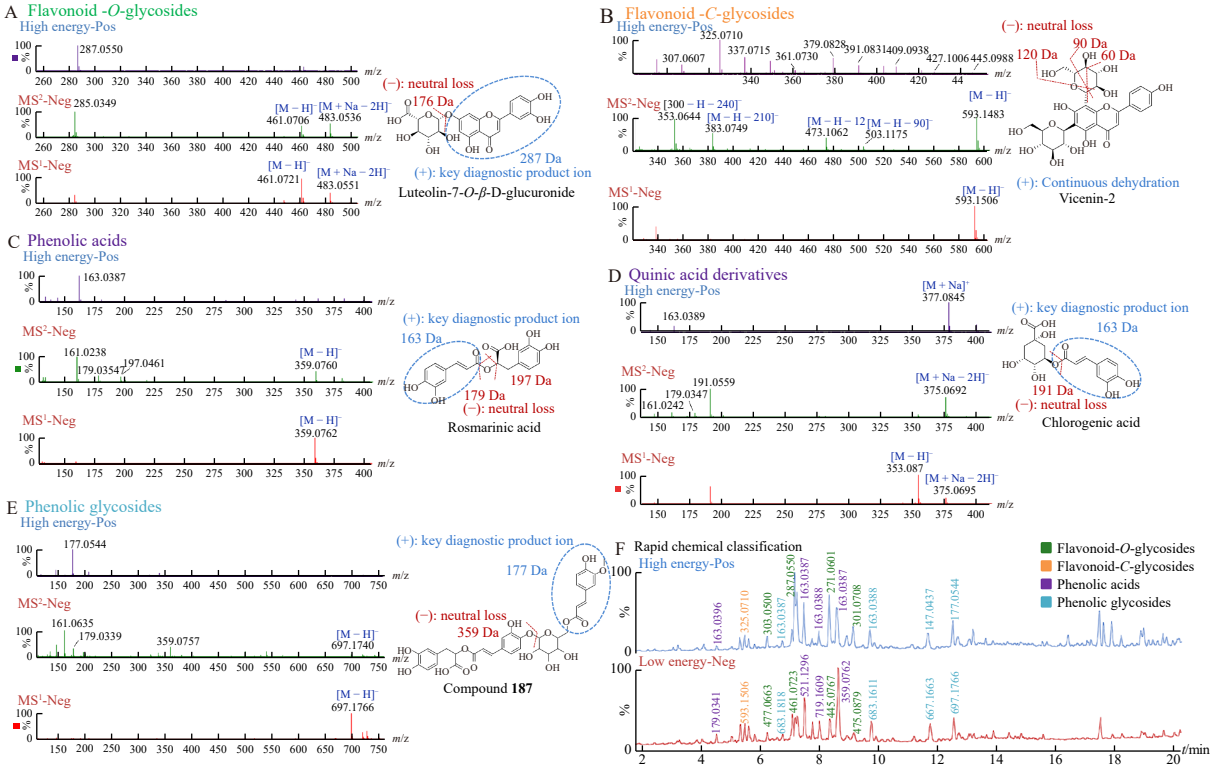

Fig. 3 Rapid chemical classification of phenolic compounds based on fragmentation patterns in negative- and positive-ion (high energy) modes. (A) MS patterns of flavonoid-*O*-glycosides in negative- and positive-ion (high energy) modes; (B) MS patterns of flavonoid-*C*-glycosides in negative- and positive-ion (high energy) modes; (C) MS patterns of phenolic acids in negative- and positive-ion (high energy) modes; (D) MS patterns of quinic acid derivatives in negative- and positive-ion (high energy) modes; (E) MS patterns of phenolic glycosides in negative- and positive-ion (high energy) modes; (F) Rapid chemical classification of phenolic compounds based on the MS patterns in negative- and positive-ion (high energy) modes.

ing between the *Elsholtzia* and *Mosla* genera.

Application to authentication in TCM-XR products

To enhance the discrimination of TCM-XR from species that are easily confused, we conducted chemometric analyses incorporating historically misidentified species (ES and EC), along with commercial TCM-XR products and the corresponding original plants (MC and MCJ). The PCA depicted in Fig. 4C illustrates that the distribution of TCM-XR products spans across various species, complicating the identification of the precise original plants. This difficulty arises from the notable differences in metabolite concentrations between the leaf and stem organs, as highlighted by the S-plot from the OPLS-DA in Figures S8A and S8B. These disparities in metabolite accumulation are further corroborated by the TIC for MC stems and leaves (Figure S8C). The PCA results, shown in Fig. 4D, which considered dried aerial parts from four species alongside TCM-XR products, revealed that commercial TCM-XR-2 and -3 products clustered with MCJ. This finding suggests that the ratio of stems to leaves in TCM-XR products significantly impacts their chemical profile and intrinsic quality. For diverse commercial products, including food items, beverages, tea-based drinks, and herbal medicines, controlling the stem-to-leaf ratio is crucial to maintain their inner quality. Moreover, the distribution of TCM-XR-1 in the PCA analysis was proximate to EC samples, indicating the potential adulteration of this batch. Additionally, the overlapping distributions of MCJ and TCM-XR in the PCA underscore that post-harvest processing minimally affects the concentration of non-volatile phenolic metabolites in TCM-XR products. This observation affirms the higher reliability of non-volatile metabolites as chemical markers for distinguishing between similar species during quality control processes (Fig. 4D).

As the designated original plant for TCM-XR, MCJ is primarily cultivated as a variant of MC in Jiangxi Province, China. Fig. 4D elucidates that the metabolic differences among the confusable species (ES, EC, MC, and MCJ) stem from variations in genera and geographic origins. Leveraging these distinct metabolic profiles, we utilized two OPLS-DA models to identify reliable chemical markers that distinguish these species based on their genera and origins (Figs. 5A and 5B). Four flavonoid glycosides (cynaroside, scutellarein-7-*O*-D-glucoside, rutin, and vicenin-2) alongside a phenolic glycoside (salviaflaside) were pinpointed as dependable chemical markers through cross-validation, considering both genera and geographic differences (Tables S6 and S7). The commercial availability of reference standards for these markers was also verified (Figs. 5C and 5D). Figs. 5E and 5F present the molecular structures and the extraction ion chromatograms (EIC) of these markers derived from three batches of TCM-XR products, as well as the four species that are commonly confused.

The semi-quantitative analysis of the five chemical markers identified in this study, illustrated in Figs. 5G and 5I, reveals significant insights into their distribution across the tested species. Notably, *Elsholtzia ciliata* (EC) exhibited a

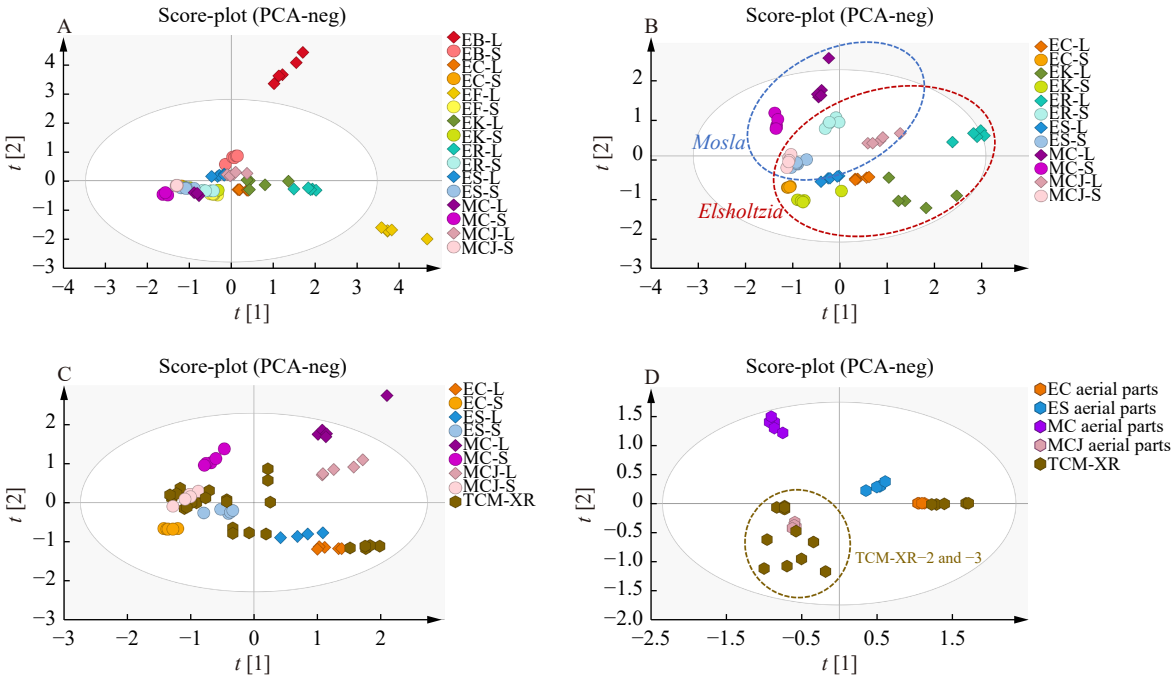

Fig. 4 The chemometric analysis of *Elsholtzia*, *Mosla* species and TCM-XR. (A) PCA analysis of leaf and stem samples of eight *Elsholtzia* and *Mosla* species in the negative-ion mode; (B) PCA analysis of leaf and stem samples of six *Elsholtzia* and *Mosla* species in the negative-ion mode (by excluding EB and EF); (C) PCA analysis of leaf and stem samples of four easily-confused species and different batches of TCM-XR in the negative-ion mode; (D) PCA analysis of aerial parts of four easily-confused species and different batches of TCM-XR in the negative-ion mode.

substantially higher concentration of cynaroside compared to the other species. Conversely, *Elsholtzia splendens* (ES) shared a closer profile with the two *Mosla* species regarding the presence of salviaflaside, while vicenin-2's relative content played a pivotal role in authenticating ES. Among the original plants of TCM-XR, MC showed higher levels of salviaflaside and rutin than MCJ. Additionally, a notable variance in the content of scutellarein-7-*O*-D-glucoside between MC and MCJ was observed (Figs. 5F and 5G). For the TCM-XR-2 and -3 products, the composition of the five chemical markers aligned more closely with MCJ, the geo-authentic cultivated species. However, the absence of salviaflaside in TCM-XR-1 suggests its counterfeit nature (Fig. 5G), indicating salviaflaside's potential as a crucial marker for authenticating TCM-XR products. Furthermore, EIC of the five chemical markers across four *Elsholtzia* species, including ER, EK, EF, and EB (Fig. 5H), revealed the absence of salviaflaside in these species, while cynaroside was present in all, underscoring its significance in authenticating *Elsholtzia* species (Fig. 5I). Therefore, the deployment of these five validated chemical markers significantly aids in distinguishing and authenticating the original TCM-XR plants from species with similar profiles, particularly emphasizing salviaflaside and cynaroside for their specific accumulation in the *Mosla* and *Elsholtzia* genera, respectively. The accessibility of commercial reference standards for these markers further facilitates the quality control and authentication of TCM-XR products, enhancing the reliability and safety of these traditional medicinal offerings.

Differential analysis of biosynthetic pathways in Elsholtzia and Mosla

Leveraging the identification of five reliable chemical markers, we undertook a differential analysis of biosynthetic pathways to uncover the underlying mechanisms responsible for the metabolic distinctions between the *Elsholtzia* and *Mosla* genera. Our investigation revealed that all five markers are products of biosynthesis pathways related to L-phenylalanine, with their relative abundances among different species and organs detailed in Fig. 6. While rosmarinic acid—a prevalent phenolic acid in both genera—was more concentrated in *Elsholtzia*, suggesting variations in rosmarinic acid content may stem from differential levels of its precursor, danshensu (Fig. 6). Conversely, salviaflaside, the corresponding glycoside of rosmarinic acid, exhibited greater abundance in the two *Mosla* species and ES. Significantly, only the *Mosla* species manifested an accumulation of a

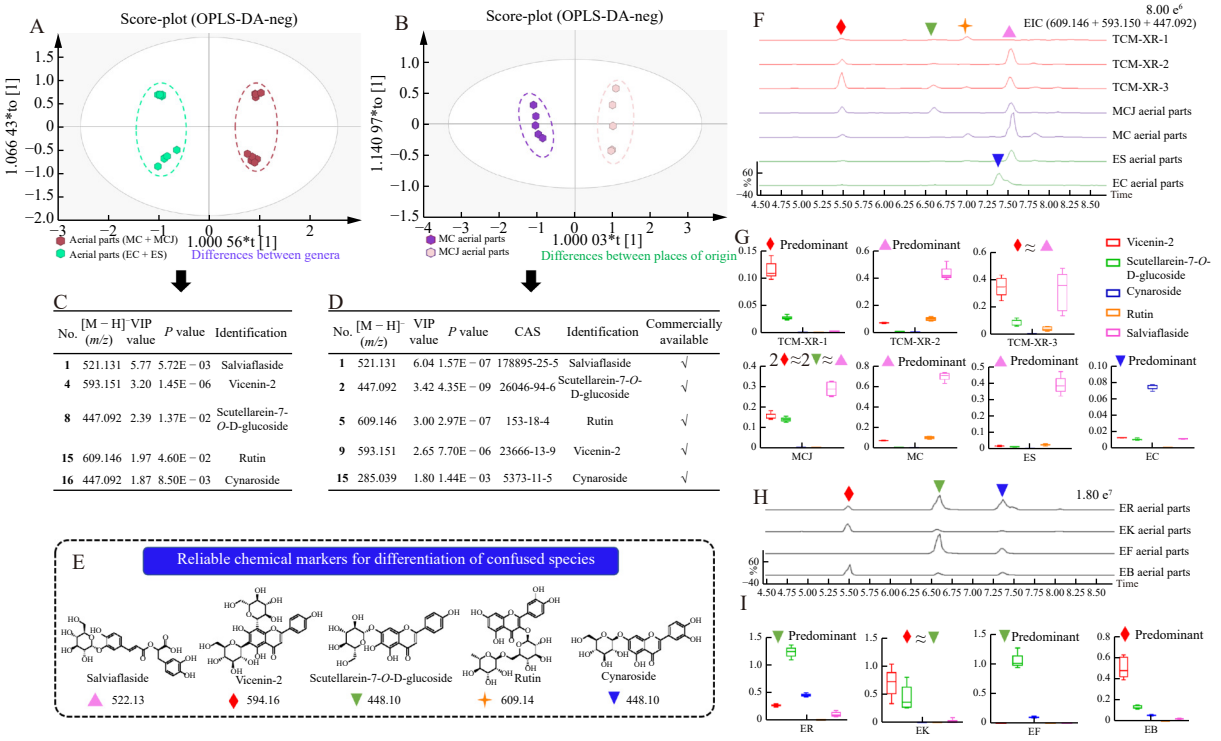

Fig. 5 Reliable chemical markers for identification of *Mosla* species and easily confused species (EC and ES). (A) OPLS-DA analysis between aerial parts of *Mosla* species and easily-confused species (EC and ES) in the negative-ion mode; (B) OPLS-DA analysis between aerial parts of MC and MCJ in the negative-ion mode; (C) Chemical markers with VIP > 1.0, $P < 0.05$ obtained from OPLS-DA analysis between aerial parts of *Mosla* species and easily-confused species (EC and ES); (D) Chemical markers with VIP > 1.0, $P < 0.05$ obtained from OPLS-DA analysis between aerial parts of MC and MCJ; (E) Structures of five reliable chemical markers; (F) Extracted ion chromatograms (EIC) of reliable chemical markers in *Mosla* TCM-XR species and confused species (EC and ES); (G) Relative content and ratio of reliable chemical markers in *Mosla* TCM-XR species and easily-confused species (EC and ES); (H) EIC of reliable chemical markers in ER, EK, EF and EB; (I) Relative content and ratio of reliable chemical markers in ER, EK, EF, and EB.

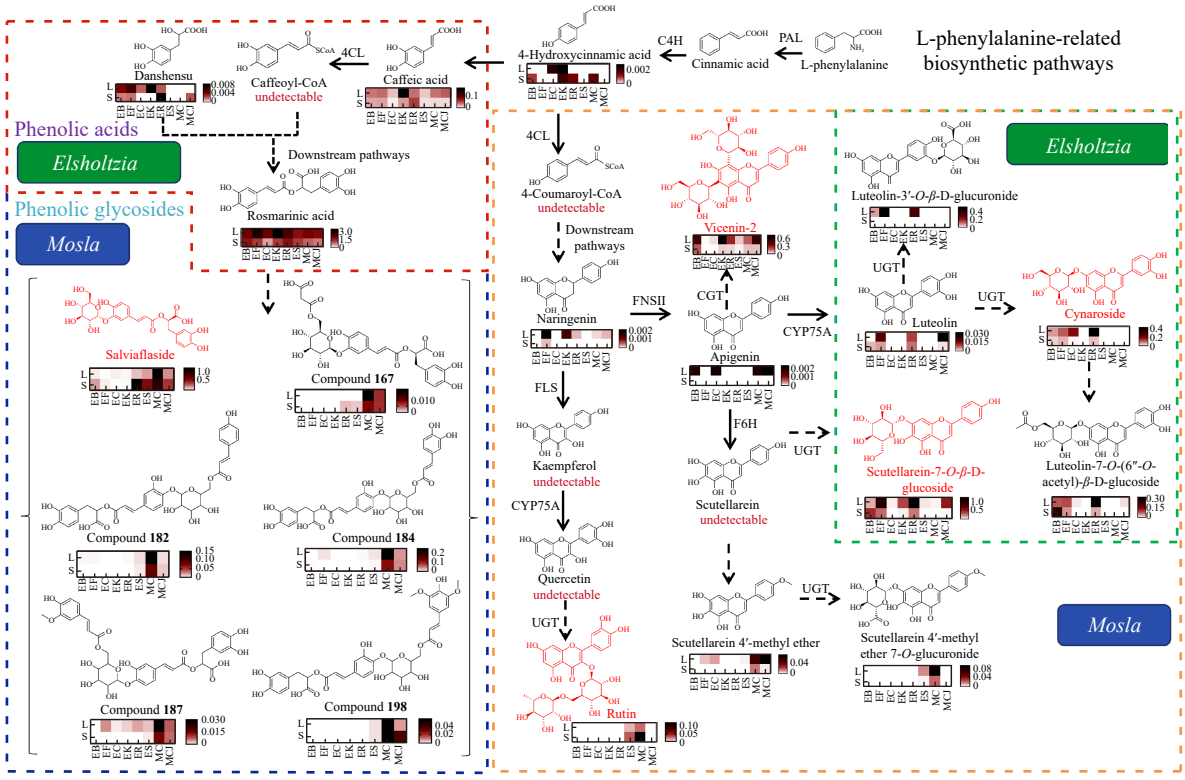

Fig. 6 Relative content of metabolic markers in the L-phenylalanine-related biosynthetic pathways in leaves and stems of eight *Elsholtzia* and *Mosla* species.

series of phenolic glycosides (compounds **165**, **179**, **181**, **184**, and **195**) featuring a salviaflaside substructure. This pattern indicates that the activity of glycosyltransferases (UGTs), utilizing phenolic acids as substrates, is potentially more pronounced in *Mosla* species (Fig. 6). Regarding the flavonoid pathways, which originate from aglycones of apigenin and quercetin, these were generally found in higher concentrations within the *Mosla*. Conversely, glycosides derived from luteolin and scutellarein were more abundant in *Elsholtzia*, while those based on the aglycone of *O*-methyl scutellarein were predominantly found in the *Mosla* (Fig. 6). This differential accumulation suggests that both *Elsholtzia* and *Mosla* serve as natural sources of distinct flavonoids, with markers like salviaflaside and luteolin glycosides serving as key discriminants between these often-confused genera. Furthermore, this analysis of biosynthetic pathways not only contributes to our understanding of the metabolic distinctions between *Elsholtzia* and *Mosla* but also lays the groundwork for future research into differential and functional gene mining.

Conclusion

In this study, we have successfully implemented a swift metabolite profiling approach for the authentication of TCM-XR against closely related *Elsholtzia* species. Utilizing a metabolomics-based method, we identified diagnostic products in positive-ion mode and employed a variety of structural reference standards for the rapid chemical characterization and classification of 203 distinct compounds. Our research highlights the pivotal role of non-volatile compounds as dependable chemical markers for distinguishing between plant species and ensuring quality control. The method developed in this research demonstrates significant potential for broader application across various plants used within the food and herbal medicine sectors, thereby contributing valuable insights and tools to the field of plant metabolomics.

Supplementary Materials

Supplementary data to this article can be obtained by sending an E-mail to the corresponding authors.

References

[1] *Pharmacopoeia of the Peoples Republic of China* [S]. Beijing: People's Medical Publishing House, 2015, 1: 271.
[2] Cao L, Si HY, Liu Y, *et al*. Essential oil composition, antimicrobial and antioxidant properties of *Mosla chinensis* maxim [J]. *Food Chem*, 2008, **115**(3): 801-805.
[3] Chen SQ, Chen JX, Xu YF, *et al*. *Elsholtzia*: a genus with antibacterial, antiviral, and anti-inflammatory advantages [J]. *J Ethnopharmacol*, 2022, **297**: 115549.
[4] Xie ZW. *Traditional Chinese Medicine Theory and Application* [M]. Beijing: People's Medical Publishing House, 2008: 916-918.
[5] *Pharmacopoeia of the Peoples Republic of China* [S]. Beijing: People's Medical Publishing House, 1997, 1: 420.
[6] *Pharmacopoeia of the Peoples Republic of China* [S]. Beijing: People's Medical Publishing House, 1985, 1: 223.
[7] *Pharmacopoeia of the Peoples Republic of China* [S]. Beijing:

People's Medical Publishing House, 1990, 1: 230.
[8] Seo YH, Trinh TA, Ryu SM, *et al*. Chemical constituents from the aerial parts of *Elsholtzia ciliata* and their protective activities on glutamate-induced HT22 cell death [J]. *J Nat Prod*, 2020, **83**(10): 3149-3155.
[9] Zhao MP, Liu XC, Lai DW, *et al*. Analysis of the essential oil of *Elsholtzia ciliate* aerial parts and its insecticidal activities against liposcelis bostrychophila [J]. *Helv Chim Acta*, 2016, **99**(1): 90-94.
[10] Peng L, Xiong Y, Wang M, *et al*. Chemical composition of essential oil in *Mosla chinensis* Maxim cv. jiangxiangru and its inhibitory effect on *Staphylococcus Aureus* biofilm formation [J]. *Open Life Sci*, 2018, **13**: 1-10.
[11] Pasdaran A, Sheikhi D. Volatile oils: potential agents for the treatment of respiratory infections [J]. *Microbiol Respir System Infect*, 2016, **16**: 237-261.
[12] Shu RG, Hu HW, Zhang PZ, *et al*. Triterpenes and flavonoids from *Mosla chinensis* [J]. *Chem Nat Compd*, 2012, **48**(4): 706-707.
[13] Nguyen D, Tran H, Schwaiger S, *et al*. Effect of non-volatile constituents of *Elsholtzia ciliata* (Thunb.) Hyl. from southern Vietnam on reactive oxygen species and nitric oxide release in macrophages [J]. *Chem Biodivers*, 2021, **18**(1): e2000577.
[14] Kalua CM, Allen MS, Bedgood Jr DR, *et al*. Olive oil volatile compounds, flavour development and quality: a critical review [J]. *Food Chem*, 2007, **100**(1): 273-286.
[15] Shimizu T, Watanabe M, Fernie AR, *et al*. Targeted LC-MS analysis for plant secondary metabolites [J]. *Methods Mol Biol*, 2018, **1778**: 171-181.
[16] Want EJ. LC-MS untargeted analysis [J]. *Methods Mol Biol*, 2018, **1738**: 99-116.
[17] Emwas AH. The strengths and weaknesses of NMR spectroscopy and mass spectrometry with particular focus on metabolomics research [J]. *Methods Mol Biol*, 2015, **1277**: 161-193.
[18] Li SL, Han QB, Qiao CF, *et al*. Chemical markers for the quality control of herbal medicines: an overview [J]. *Chin Med*, 2008, **3**: 7.
[19] Xiong QQ, Sun CH, Li A, *et al*. Metabolomics and biochemical analyses revealed metabolites imp ortant for the antioxidant properties of purple glutinous rice [J]. *Food Chem*, 2022, **389**: 133080.
[20] Tsugawa H, Cajka T, Kind T, al. MS-DIAL: data-independent MS/MS deconvolution for comprehensive metabolome analysis [J]. *Nat Methods*, 2015, **12**(6): 523-526.
[21] Fraisier-Vannier O, Chervin J, Cabanac G, *et al*. MS-CleanR: a feature-filtering workflow for untargeted LC-MS based metabolomics [J]. *Anal Chem*, 2020, **92**(14): 9971-9981.

Cite this article as: ZENG Zhen, ZHANG Chen, HU Jiadong, WANG Feiyan, WU Ziding, WANG Jing, ZHANG Jun, YANG Shuda, CHEN Junfeng, LI Mingming, TONG Qi, QIU Shi, CHEN Wansheng. Rapid characterization of non-volatile phenolic compounds reveals the reliable chemical markers for authentication of traditional Chinese medicine Xiang-ru among confusing *Elsholtzia* species [J]. *Chin J Nat Med*, 2024, **22**(4): 375-384.